NANO LETTERS

Letter

pubs.acs.org/NanoLett

Charge Percolation Pathways Guided by Defects in Quantum Dot Solids

Yingjie Zhang,[†,‡] Danylo Zherebetskyy,[‡] Noah D. Bronstein,[§] Sara Barja,[‡] Leonid Lichtenstein,[‡] David Schuppisser,[‡] Lin-Wang Wang,[‡] A. Paul Alivisatos,[‡,§,∥,⊥] and Miquel Salmeron*[,‡,∥]

[†]Applied Science and Technology Graduate Program, University of California at Berkeley, Berkeley, California 94720, United States

[‡]Materials Sciences Division, Lawrence Berkeley National Laboratory, Berkeley, California 94720, United States

[§]Department of Chemistry, University of California at Berkeley, Berkeley, California 94720, United States

[∥]Department of Materials Science and Engineering, University of California at Berkeley, Berkeley, California 94720, United States

[⊥]Kavli Energy NanoScience Institute, Berkeley, California 94720, United States

Supporting Information

ABSTRACT: Charge hopping and percolation in quantum dot (QD) solids has been widely studied, but the microscopic nature of the percolation process is not understood or determined. Here we present the first imaging of the charge percolation pathways in two-dimensional PbS QD arrays using Kelvin probe force microscopy (KPFM). We show that under dark conditions electrons percolate via in-gap states (IGS) instead of the conduction band, while holes percolate via valence band states. This novel transport behavior is explained by the electronic structure and energy level alignment of the individual QDs, which was measured by scanning tunneling spectroscopy (STS). Chemical treatments with hydrazine can remove the IGS, resulting in an intrinsic defect-free semiconductor, as revealed by STS and surface potential spectroscopy. The control over IGS can guide the design of novel electronic devices with impurity conduction, and photodiodes with controlled doping.

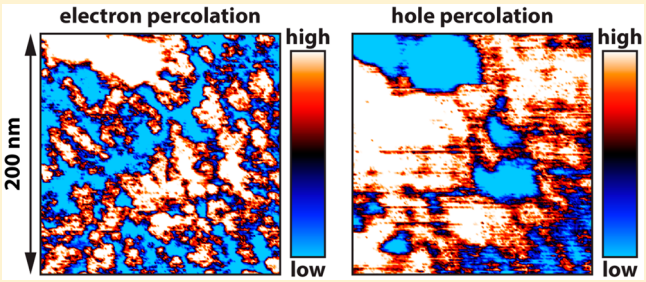

KEYWORDS: *Quantum dot, charge transport, charge percolation, defect, in-gap states, Kelvin probe force microscopy*

An important goal in the design of modern materials is to create new forms of matter by combining elementary nanoscale building blocks.[1−9] One example is the artificial solids formed by placing quantum dots in arrays.[4−9] By controlling the band gap of the individual dots through their size, and the degree to which charges move from one dot to the next through controlled barriers, we can design and tune the transport properties of quantum dot solids. Potential applications include solution-processed field effect transistors, solar cells, photodetectors, etc.[4−9] The individual QDs are themselves complex, tiny solids, comprised of hundreds to thousands of atoms. Inevitably the fabrication of these constituents is imperfect; consequently, the QDs are not identical in the number and arrangement of atoms. In addition, defects and impurities are also present that can play an important role.[10−13] Therefore, it is not surprising that the microscopic mechanisms of charge hopping in QD arrays have not yet been determined.[7,8,13−17]

Understanding the transport mechanism is also relevant to a broader class of disordered semiconductors,[18] which are systems with spatial disorder and/or heterogeneity in the electronic states. Examples include amorphous silicon,[19] heavily doped and highly compensated semiconductors,[20] and organic semiconductors.[21] These systems exhibit spatially varying potential energy landscapes, which are determined by the microscopic disorder, the energy level alignment of individual sites, and the strength of coupling between adjacent sites. When charges are injected, they will fill the potential valleys, forming percolation pathways.[22] As a model system, quantum dot solids offer a unique opportunity for local characterization of the individual building blocks, whose properties can be correlated with the mesoscale percolation and ensemble transport phenomena.

Here we combined scanning tunneling microscopy (STM), Kelvin probe force microscopy (KPFM), and field effect transistor (FET) techniques to characterize the states responsible for charge percolation in QD solids both microscopically and spectroscopically. We found a phenomenon where in-gap states (IGS) induce Fermi level pinning favoring electron transport via the conductive IGS, forming percolation pathways. Both the technical methodology and the determined transport mechanism can be generally applicable to other disordered semiconductors.

Received: February 3, 2015
Revised: April 1, 2015

ACS Publications © XXXX American Chemical Society

DOI: 10.1021/acs.nanolett.5b00454
Nano Lett. XXXX, XXX, XXX−XXX

Direct Imaging of Charge Transport in PbS Quantum Dots. We chose PbS QDs as the artificial atoms from which to form artificial solids, in the form of thin films consisting of 0−2 QD layers. These QDs show strong quantum confinement due to the large Bohr radius,[23] so that the wave function of one dot can extend into neighboring dots, giving rise to an electrically active QD solid. As-synthesized PbS QDs (5.5 nm diameter, ∼0.9 eV band gap, Supporting Information) are capped with insulating oleate ligands[24] that can be exchanged with shorter ligands, such as 1,2-ethanedithiol (EDT), 3-mercaptopropionic acid (MPA), iodide, etc., to couple the QDs and enhance conduction.[5,6,12−15]

To resolve the spatial and energetic pathways of electron and hole transport, we used KPFM[25,26] to quantitatively image the local surface potential (V_{sf}) distribution in a QD film deposited in the channel region of a field effect transistor (FET) (Figure 1A). All KPFM and FET measurements were done under dark conditions in an inert atmosphere. The QDs were treated with EDT (labeled PbS-EDT). The oxide surface in the FET channel region was passivated by a layer of octadecyltrichlorosilane (OTS) to remove charge traps at the oxide surface (Supporting Information). The sign of V_{sf} is set such that $E = eV_{sf}$, where e is the absolute value of the elementary charge, and E is the Fermi level position relative to vacuum. To image the charge percolation pathways we functionalized the KPFM tip with PbS QDs (Supporting Information), resulting in ∼10 nm spatial resolution. To distinguish conductive from nonconductive regions we applied a high gate bias (V_g = ±52 V) to inject ∼1 elementary charge per QD into the channel (with source/drain electrodes grounded). The surface potential along the percolation pathways will be pinned by the energy levels responsible for charge transport. The areas with no conductive states at the corresponding energy will exhibit higher (for electrons) or lower (for holes) surface potential due to gate field penetration. The topographic image shows the distribution of individual PbS-EDT QDs in a channel area (Figure 1B), while the surface potential images of the same area (Figure 1C, D) reveal the transport pathway structures. The electron percolation pathways, shown by the cyan/blue areas in Figure 1C (where the injected electrons reside), are in the form of narrow stripes surrounded by electron-insulating areas (red/white). In contrast, the hole percolation pathways, shown by the white/red areas in Figure 1D (where the injected holes reside), form larger domains surrounded by hole-insulating areas (blue/cyan). The hole transporting level is located at ∼−5.0 eV (below vacuum level), matching the valence band edge position of the QDs.[27] However, the level responsible for electron transport is located at ∼−4.8 eV, far below the conduction band edge (∼−4.1 eV). The presence of electron-conducting IGS at ∼−4.8 eV is an unexpected finding.

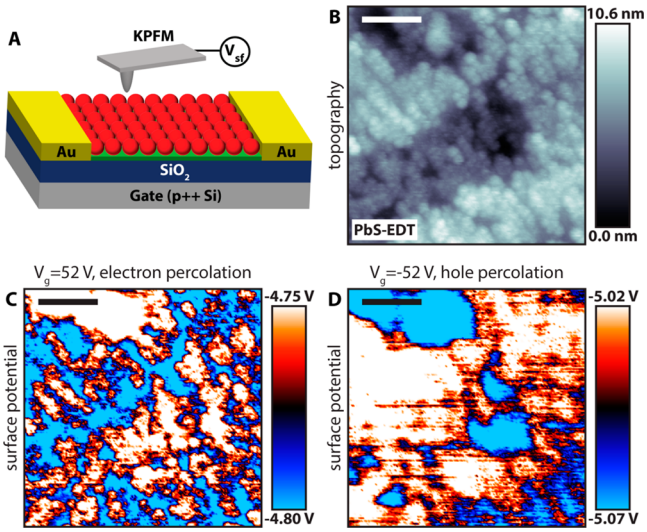

Figure 1. Imaging charge percolation pathways in QD solids. (A) Schematic diagram of a QD thin film FET and KPFM probe setup. Au electrodes serve as the source and drain. The FET channel length is 20 μm, and its width is 1 mm. A monolayer of OTS (green) was preadsorbed on the SiO_2 surface of the channel to passivate the oxide surface trap states. (B to D) KPFM images of the same region in the channel area of a PbS-EDT QD array FET. Scale bar: 50 nm. (B) Topography showing 0−2 layers of QD, (C and D) surface potential maps at V_g = 52 V and V_g = −52 V, respectively. Source and drain electrodes were grounded during measurements. The color scales of the surface potential images are saturated to enhance contrast. The same images with nearly the full scales show the same percolation pathway structures (Supporting Information).

In-Gap States and Charge Percolation Mechanism. To better understand the percolation phenomena, we measured the electronic structure of individual QDs using STM and scanning tunneling spectroscopy (STS) (Figure 2A, B). Measurements were done at 77 K in ultrahigh vacuum (base pressure <10^{-10} mbar). STS was performed to obtain density of states (DOS) spectra on 30 randomly chosen QDs deposited on an indium tin oxide (ITO) substrate. Three different kinds of spectra were observed (Figure 2C). About one-half of the spectra (type 1) show peaks due to IGS at ∼0.05−0.1 eV above the Fermi level, and $1S_h$ states (valence band) at ∼0.1−0.25 eV below the Fermi level. Type 2 and type 3 spectra (similar amount) show no IGS. Type 2 spectra have the $1S_h$ states in the same range as type 1 spectra, whereas type 3 spectra have $1S_h$ states at ∼0.25−0.45 eV below the Fermi level. The origin of the IGS will be discussed later.

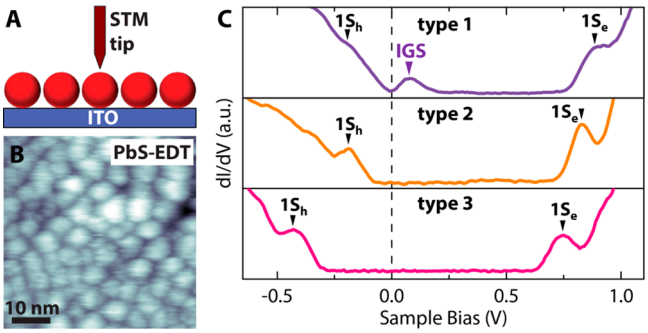

Figure 2. Electronic structure of individual PbS-EDT quantum dots. (A) Schematic diagram of STM and STS measurements of QDs deposited on an ITO substrate. (B) STM image with individually resolved PbS-EDT QDs. (C) STS curves of individual PbS-EDT QDs. The sample bias corresponds to the energy level position with respect to Fermi level. Three types of spectra are found, labeled according to the existence of in-gap states (IGS) and to $1S_h$ level alignment.

The observed conductivity of the IGS implies that they are partially delocalized to facilitate electron hopping from one IGS to the next. Since the IGS are empty states near the valence band, they induce p-type doping and pin the Fermi level in the ∼0.2 eV gap between the IGS and $1S_h$ states. Since the type 2 spectra show p-type doping (Fermi level close to $1S_h$ states),

DOI: 10.1021/acs.nanolett.5b00454
Nano Lett. XXXX, XXX, XXX−XXX

they likely correspond to QDs with IGS whose wave function does not extend to the top surface and thus cannot be detected by the STM tip. The three types of STS spectra found on the QD solid indicates three types of QDs (Figure 3A): type 1 QDs

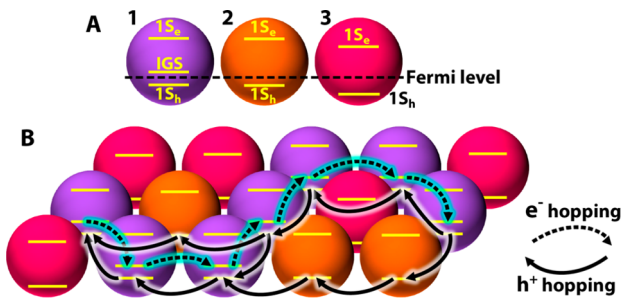

Figure 3. (A) Schematic diagram of the energy level alignment in the three types of QDs. (B) Schematic diagram illustrating the charge percolation pathways through 2-D arrays of PbS-EDT QDs. Electrons percolate through the IGS of type 1 QDs (dashed arrows), while holes hop via $1S_h$ states of type 1 and type 2 QDs (solid arrows).

have enough IGS to form a conduction pathway; type 2 QDs have some amount of IGS so that the Fermi level is close to the valence band, but their wave functions do not overlap sufficiently to provide a conductive path; type 3 QDs have no or few IGS, and their Fermi level is farther away from the valence band. These three types of QDs are related with the three types of STS spectra, but not necessarily one-to-one correlated. When the QDs are randomly packed, electrons can hop via the IGS of type 1 QDs due to proper energy level alignment. Holes on the other hand can hop through the $1S_h$ state of most of type 1 and type 2 QDs. Type 3 QDs are electronically inactive, since they have no states near the Fermi level. The percolation pathway diagram for electrons and holes then resembles that shown schematically in Figure 3B, which illustrates how the Fermi level pins at $1S_h$ states or at IGS when holes or electrons are injected, respectively. It also shows that the hole percolation domains are different, and spatially larger, than those of electrons, in agreement with the experimental surface potential maps. The spatially connected patchy pathway structures resemble that of resistor networks, which have long been predicted by percolation theory.[28]

We note that this IGS-induced Fermi level pinning is a general phenomenon occurring in all kinds of semiconductors.[29] Therefore, percolation through IGS is energetically favored for at least one type of carriers if the defect concentration is sufficiently high to induce significant wave function overlap of adjacent IGS. QD solids, with their porous structure and larger surface area, are thus inherently suitable for engineering impurity conduction via chemical treatments.

Conduction Channel Switching and Intrinsic Quantum Dots. While a sufficient amount of IGS is beneficial for electron transport in QD solids under dark conditions, in photodiodes designed for transport of photoexcited charge carriers via valence/conduction bands, the deep IGS can act as recombination centers resulting in loss of efficiency. Previous studies showed that hydrazine (HYD) acts to increase the mobility of lead chalcogenide QDs which might be partially due to the removal of defect states.[7] We thus performed HYD treatments to modulate the amount of IGS. We performed STS measurements on 43 individual HYD treated QDs (labeled PbS-HYD) and found that all of them have a clean band gap with the Fermi level near the midgap (Figure 4B). This reveals that HYD is effective in removing the IGS, resulting in intrinsic

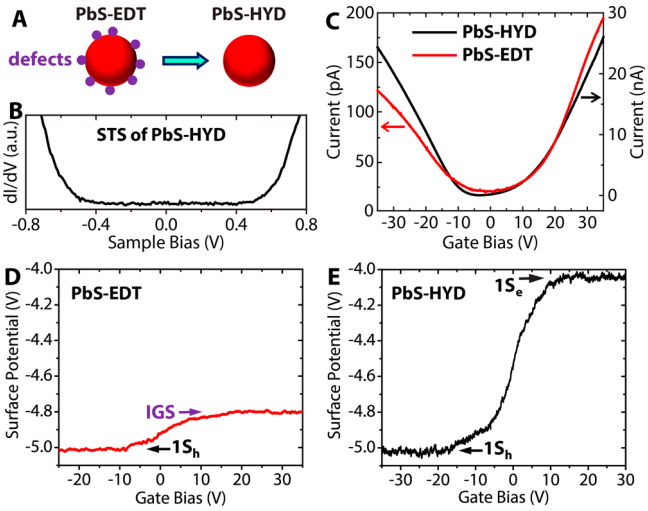

Figure 4. Surface defect engineering via chemical treatments. (A) Schematic diagram with surface defects present on PbS-EDT QDs but absent on PbS-HYD QDs. (B) STS curve of a PbS-HYD QD showing a clean band gap with the Fermi level in the midgap. (C) Transfer curves from PbS-EDT and PbS-HYD QD thin film FETs, with a drain bias of −5 V. (D and E) Surface potential−gate bias spectra of the EDT and HYD treated samples. The surface potential is plotted in the same scale in the two figures.

QDs. The quantum confined peaks are smeared out in the dI/dV curve, but are evident after spectra renormalization (Supporting Information).

To compare the charge transport properties of the QDs with and without IGS, we measured the source−drain current (I_d) versus gate bias curves (transfer curves) of PbS-EDT and PbS-HYD QD thin film FETs, with a small bias $V_d = -5$ V applied to the drain and with the source grounded. The slope in the linear part of the curves (Figure 4C) is proportional to the carrier mobility in the states involved in the transport.[29] We can see that the EDT and HYD treated QD arrays are both ambipolar, with electron conduction at positive gate bias, and hole conduction at negative gate bias. PbS-HYD shows similar electron (μ_e) and hole mobility (μ_h), while PbS-EDT shows $\mu_e \approx 2.2\ \mu_h$. The electronic levels involved in charge transport can also be measured with KPFM by means of surface potential (V_{sf})−gate bias (V_g) spectroscopy[25] with the tip placed above the QDs (Figure 4D, E), with source and drain electrodes grounded. The curves in Figure 4D show that, for PbS-EDT, V_{sf} is pinned by the $1S_h$ states and by the IGS, in agreement with the proposed mechanism of hole transport via the $1S_h$ state and electron transport via IGS. The larger electron mobility (compared to hole mobility) indicates good coupling of IGS between QDs. In contrast, the curves in Figure 4E reveal that V_{sf} is pinned by the $1S_h$ and $1S_e$ states (conduction band) at high negative/positive gate bias, respectively. The nearly linear transition of the surface potential from the $1S_h$ to $1S_e$ states also confirmes the absence of IGS.[25] This is in agreement with the STS and transport results, confirming that hole transport occurs via $1S_h$ states while electron transport occurs via $1S_e$ states in the case of PbS-HYD. For PbS QDs the electrons in the $1S_e$ state and the holes in the $1S_h$ state have the same effective mass,[23] resulting in similar mobility. KPFM imaging of PbS-HYD at $V_g = \pm 52$ V reveals that the electron and hole follow

DOI: 10.1021/acs.nanolett.5b00454
Nano Lett. XXXX, XXX, XXX−XXX

the same pathways (Supporting Information), further confirming the conduction/valence band transport mechanism.

The electron/hole mobility in the localized hopping transport regime depends not only on the percolation domain size but also on the electronic coupling of neighboring states (β), dispersion of state energy ($\Delta\alpha$), and Coulomb charging energy (E_c).[7,30] For lead chalcogenide nanocrystals, E_c is typically small and can be neglected at room temperature.[7,23] β depends on the localization of the transport states and the distance between neighboring states, which is hard to quantify for the IGS. As to $\Delta\alpha$, STS results show that the $1S_h$ state is more dispersed than the IGS for the PbS-EDT QDs. A smaller $\Delta\alpha$ could be responsible for the fact that $\mu_e > \mu_h$ for the 2-D PbS-EDT arrays studied here. From comparison of PbS-HYD and PbS-EDT QDs, the former have a much higher surface coverage (95% vs 59%, as determined from AFM images), and a larger β due to the smaller interparticle distance (since the PbS-HYD QD surface is almost bare, as revealed by infrared absorption measurements). These two factors are responsible for the larger measured μ_e and μ_h of PbS-HYD compared to those of PbS-EDT. The submonolayer coverage is responsible for the much smaller source−drain current compared to that of thin films (typically ∼50 nm thick).

Discussion and Conclusion. There has been many postulations regarding the atomic origin of IGS in lead chalcogenide QDs, including incomplete ligand passivation,[31] nonstoichiometry,[32,33] and surface oxidation.[34−36] Here we found that hydrazine, a strong reducing agent, can efficiently remove IGS. Our results thus indicate that oxygen-related species are likely at the origin of the conductive IGS, although we cannot rule out other possibilities. We also note that there may exist shallow trap states within the thermal energy from the valence/conduction band edge, which cannot be distinguished from the $1S_h/1S_e$ states due to the resolution limit of the STM and KPFM.

The phenomenon of ambipolar transport with larger electron mobility has also been reported for PbSe QD thin films treated with EDT.[15,36] Therefore, we expect the mechanism of electron transport through IGS to be generally applicable to lead chalcogenide QD solids with EDT treatments under dark conditions in an FET geometry.

One promising application of QD solids is in large area, flexible electronics, such as transistors, circuits, memory, and sensors.[37] These devices can be fabricated by room temperature, roll-to-roll solution processing, which reduces cost. However, the fabricated QD films are more prone to defects and impurities compared to traditional high-temperature, vacuum processed crystalline semiconductors. In contrast to the traditional view that defects act simply as traps hindering carrier transport, this work shows the beneficial role of impurities, which can thus serve as the starting point for engineering conductive impurities that can be controlled during solution processing. The mechanism of in-gap state induced Fermi level pinning and favorable charge percolation via IGS is likely to be relevant to other QD and organic semiconductor systems as well.

On the other hand, for QD based optoelectronic devices in diode geometries, the goal is to harness the photoexcited charge carriers that are transported via conduction/valence band states. In contrast to the (quasi-)equilibrium process of electrostatic field-controlled charge injection and transport in the linear regime in the FETs, photocarrier transport in diodes are inherently a nonequilibrium process that requires constant pumping of carriers into valence/conduction band states. In the latter case, conduction through IGS is unlikely since electrons in IGS would quickly recombine with holes in the $1S_h$ states due to their small energy level separation (0.2 eV). But electrons in the $1S_e$ states would be able to travel (through drift and diffusion) a finite distance (100−300 nm) before recombination with IGS or $1S_h$ states.[5,6,9,31,38,39] Solar cell measurements using our PbS-EDT QDs provide an open-circuit voltage larger than 0.2 eV (not shown here), confirming that photoexcited electron transport occurs through the conduction band.

Considering that PbS-HYD was found to be intrinsic with no deep IGS, it is likely that these QDs would have a low photocarrier recombination rate and a large carrier diffusion length. Therefore, by designing p-i-n photodiodes with PbS-HYD as the intrinsic layer, we may be able to achieve much higher efficiencies in solar cells and photodetectors.[38,39]

■ ASSOCIATED CONTENT

Supporting Information

Nanocrystal synthesis and film preparation, FET preparation, KPFM measurements, KPFM images of PbS-EDT in full scale, KPFM images of PbS-HYD, normalized STS curve of PbS-HYD, contact resistance analysis. This material is available free of charge via the Internet at http://pubs.acs.org.

■ AUTHOR INFORMATION

Corresponding Author

*E-mail: mbsalmeron@lbl.gov.

Notes

The authors declare no competing financial interest.

■ ACKNOWLEDGMENTS

The authors thank Q. Chen for discussion of the manuscript. We also thank J. M. Lucas for nanocrystal synthesis and A. Pun for OTS deposition. We thank E. H. Sargent for discussion on photovoltaic applications. This work was supported by the "Self-Assembly of Organic/Inorganic Nanocomposite Materials" program, Office of Science, the Office of Basic Energy Sciences (BES), Materials Sciences and Engineering (MSE) Division of the U.S. Department of Energy (DOE) under Contract No. DE-AC02-05CH11231. It used resources of the Molecular Foundry, a DOE Office of Science user facility. S.B. acknowledges fellowship support by the European Union under FP7-PEOPLE-2012-IOF-327581. L.L. acknowledges support from the Alexander van Humboldt Foundation.

■ REFERENCES

(1) Huynh, W. U.; Dittmer, J. J.; Alivisatos, A. P. *Science* **2002**, *295*, 2425−2427.
(2) Cui, Y.; Lieber, C. M. *Science* **2001**, *291*, 851−853.
(3) Tessler, N.; Medvedev, V.; Kazes, M.; Kan, S.; Banin, U. *Science* **2002**, *295*, 1506−1508.
(4) Graetzel, M.; Janssen, R. A. J.; Mitzi, D. B.; Sargent, E. H. *Nature* **2012**, *488*, 304−312.
(5) Chuang, C. M.; Brown, P. R.; Bulović, V.; Bawendi, M. G. *Nat. Mater.* **2014**, *13*, 786−801.
(6) Ning, Z.; Voznyy, O.; Pan, J.; Hoogland, S.; Adinolfi, V.; Xu, J.; Li, M.; Kirmani, A. R.; Sun, J.-P.; Minor, J.; Kemp, K. W.; Dong, H.; Rollny, L.; Labelle, A.; Carey, G.; Sutherland, B.; Hill, I.; Amassian, A.; Liu, H.; Tang, J.; Bakr, O. M.; Sargent, E. H. *Nat. Mater.* **2014**, *13*, 822−828.
(7) Talapin, D. V.; Murray, C. B. *Science* **2005**, *310*, 86−89.

DOI: 10.1021/acs.nanolett.5b00454
Nano Lett. XXXX, XXX, XXX−XXX

(8) Lee, J.; Kovalenko, M. V.; Huang, J.; Chung, D. S.; Talapin, D. V. *Nat. Nanotechnol.* **2011**, *6*, 348−352.
(9) Clifford, J. P.; Konstantatos, G.; Johnston, K. W.; Hoogland, S.; Levina, L.; Sargent, E. H. *Nat. Nanotechnol.* **2009**, *4*, 40−44.
(10) Wolkin, M. V.; Jorne, J.; Fauchet, P. M.; Allan, G.; Delerue, C. *Phys. Rev. Lett.* **1999**, *82*, 197−200.
(11) Cordones, A. A.; Scheele, M.; Alivisatos, A. P.; Leone, S. R. *J. Am. Chem. Soc.* **2012**, *134*, 18366−18373.
(12) Diaconescu, B.; Padilha, L. A.; Nagpal, P.; Swartzentruber, B. S.; Klimov, V. I. *Phys. Rev. Lett.* **2013**, *110*, 127406.
(13) Nagpal, P.; Klimov, V. I. *Nat. Commun.* **2011**, *2*, 486.
(14) Jeong, K. S.; Tang, J.; Liu, H.; Kim, J.; Schaefer, A. W.; Kemp, K.; Levina, L.; Wang, X. H.; Hoogland, S.; Debnath, R.; Brzozowski, L.; Sargent, E. H.; Asbury, J. B. *ACS Nano* **2012**, *6*, 89−99.
(15) Liu, Y.; Gibbs, M.; Puthussery, J.; Gaik, S.; Ihly, R.; Hillhouse, H. W.; Law, M. *Nano Lett.* **2010**, *10*, 1960−1969.
(16) Bozyigit, D.; Volk, S.; Yarema, O.; Wood, V. *Nano Lett.* **2013**, *13*, 5284−5288.
(17) Drndić, M.; Markov, R.; Jarosz, M. V.; Bawendi, M. G.; Kastner, M. A.; Markovic, N.; Tinkham, M. *Appl. Phys. Lett.* **2003**, *83*, 4008−4010.
(18) Anderson, P. W. *Phys. Rev.* **1958**, *109*, 1492−1605.
(19) Le Comber, P. G.; Spear, W. E. *Phys. Rev. Lett.* **1970**, *25*, 509−511.
(20) Mott, N. F.; Twose, W. D. *Adv. Phys.* **1961**, *10*, 107−163.
(21) Coropceanu, V.; Cornil, J.; da Silva, D. A.; Olivier, Y.; Silbey, R.; Bredas, J. L. *Chem. Rev.* **2007**, *107*, 926−952.
(22) Elliott, R. J.; Krumhansl, J. A.; Leath, P. L. *Rev. Mod. Phys.* **1974**, *46*, 465−543.
(23) Kang, I.; Wise, F. W. *J. Opt. Soc. Am. B* **1997**, *14*, 1632−1646.
(24) Zherebetskyy, D.; Scheele, M.; Zhang, Y.; Bronstein, N.; Thompson, C.; Britt, D.; Salmeron, M.; Alivisatos, P.; Wang, L.-W. *Science* **2014**, *344*, 1380−1384.
(25) Zhang, Y.; Ziegler, D.; Salmeron, M. *ACS Nano* **2013**, *7*, 8258−8265.
(26) Zhang, Y.; Pluchery, O.; Caillard, L.; Lamic-Humblot, A.-F.; Casale, S.; Chabal, Y. J.; Salmeron, M. *Nano Lett.* **2015**, *15*, 51−55.
(27) Jasieniak, J.; Califano, M.; Watkins, S. E. *ACS Nano* **2011**, *5*, 5888−5902.
(28) Kirkpatrick, S. *Rev. Mod. Phys.* **1973**, *45*, 574−588.
(29) Sze, S. M. *Physics of Semiconductor Devices*, 2nd ed.; Wiley: New York, 1981.
(30) Remacle, F.; Levine, R. D. *ChemPhysChem* **2001**, *2*, 20−36.
(31) Ip, A. H.; Thon, S. M.; Hoogland, S.; Voznyy, O.; Zhitomirsky, D.; Debnath, R.; Levina, L.; Rollny, L. R.; Carey, G. H.; Fischer, A.; Kemp, K. W.; Kramer, I. J.; Ning, Z. J.; Labelle, A. J.; Chou, K. W.; Amassian, A.; Sargent, E. H. *Nat. Nanotechnol.* **2012**, *7*, 577−582.
(32) Kim, D.; Kim, D.-H.; Lee, J.-H.; Grossman, J. C. *Phys. Rev. Lett.* **2013**, *110*, 196802.
(33) Oh, S. J.; Berry, N. E.; Choi, J.-H.; Gaulding, E. A.; Paik, T.; Hong, S.-H.; Murray, C. B.; Kagan, C. R. *ACS Nano* **2013**, *7*, 2413−2421.
(34) Leschkies, K. S.; Kang, M. S.; Aydil, E. S.; Norris, D. J. *J. Phys. Chem. C* **2010**, *114*, 9988−9996.
(35) Zarghami, M. H.; Liu, Y.; Gibbs, M.; Gebremichael, E.; Webster, C.; Law, M. *ACS Nano* **2010**, *4*, 2475−2485.
(36) Luther, J. M.; Law, M.; Song, Q.; Perkins, C. L.; Beard, M. C.; Nozik, A. J. *ACS Nano* **2008**, *2*, 271−280.
(37) Kim, D. K.; Lai, Y.; Diroll, B. T.; Murray, C. B.; Kagan, C. R. *Nat. Commun.* **2012**, *3*, 1216.
(38) Zhitomirsky, D.; Voznyy, O.; Levina, L.; Hoogland, S.; Kemp, K. W.; Ip, A. H.; Thon, S. M.; Sargent, E. H. *Nat. Commun.* **2014**, *5*, 3803.
(39) Engel, J. H.; Alivisatos, A. P. *Chem. Mater.* **2014**, *26*, 153−162.

DOI: 10.1021/acs.nanolett.5b00454
Nano Lett. XXXX, XXX, XXX−XXX